Multi frame synchrotron radiography of pulsed power driven underwater single wire explosions

D. Yanuka,[1] A. Rososhek,[2] S. Theocharous,[1] S. N. Bland,[1] Ya. E. Krasik,[2] M. P. Olbinado,[3] and A. Rack[3]

[1]*Plasma Physics Group, Imperial College London, London SW7 2BW, United Kingdom*
[2]*Physics Department, Technion - Israel Institute of Technology, Haifa 32000, Israel*
[3]*European Synchrotron Radiation Facility, CS40220, 38043 Grenoble Cedex 9, France*

We present the first use of synchrotron-based phase contrast radiography to study pulsed-power driven high energy density physics experiments. Underwater electrical wire explosions have become of interest to the wider physics community due to their ability to study material properties at extreme conditions and efficiently couple stored electrical energy into intense shock waves in water. The latter can be shaped to provide convergent implosions, resulting in very high pressures (1-10 Mbar) produced on relatively small pulsed power facilities (100s of kA-MA). Multiple experiments have explored single-wire explosions in water, hoping to understand the underlying physics and better optimize this energy transfer process; however, diagnostics can be limited. Optical imaging diagnostics are usually obscured by the shock wave itself; and until now, diode-based X-ray radiography has been of relatively low resolution and rather a broad x-ray energy spectrum. Utilising phase contrast imaging capabilities of the ID19 beamline at the European Synchrotron Radiation Facility, we were able to image both the exploding wire and the shock wave. Probing radiation of 20-50 keV radiographed 200 μm tungsten and copper wires, in ∼2-cm diameter water cylinders with resolutions of 8 μm and 32 μm. The wires were exploded by a ∼30-kA, 500-ns compact pulser, and 128 radiographs, each with a 100-ps X-ray pulse exposure, spaced at 704 ns apart were taken in each experiment. Abel inversion was used to obtain the density profile of the wires, and the results are compared to two dimensional hydrodynamic and one dimensional magnetohydrodynamic simulations. *Published by AIP Publishing.* https://doi.org/10.1063/1.5047204

I. INTRODUCTION

Underwater electrical wire explosions have drawn much attention for the last 60 years due to their use in exploring the Equations of State (EOS) and electrical conductivity of materials, and for potential industrial applications including mining and fracking for the petroleum industry.[1–7] Due to a high electric field breakdown threshold in water (>200 kV/cm), plasma formation along the wire's surface, which dominates wire explosions in vacuum or gas, is prevented. Furthermore, water's small compressibility allows one to keep high energy density deposition into the exploding wire.

When energy is delivered to a wire in a water cell, the wire experiences rapid solid-liquid-vapor-plasma transitions. The latter phase is a weakly-ionized plasma with a rather large resistivity allowing one to obtain an overdamped discharge during which almost all preliminary stored energy is delivered to the exploding wire. The liquid-gas-plasma transition is characterised by a fast decrease in the discharge current and subsequently in self-magnetic field pressure. This phase of the wire explosion is accompanied by the wire's radial expansion with a velocity significantly exceeding the sound velocity in non-disturbed water, thus generating strong shock waves with good coupling (∼24%) of the energy between the amount stored in the capacitors to the water flow behind the shock.[8,9] Recently the use of underwater electrical explosions of cylindrical and spherical arrays of wires in water has drawn further interest, as the shock waves from adjacent wires can merge, resulting in highly efficient convergent implosions producing high pressure warm dense matter conditions in the vicinity of the implosion axis or origin.[10,11]

Some of the methods used for the diagnostics of underwater electrical wire explosions include optical spectroscopy, optical shadow imaging, and piezo based pressure probes. These can provide useful information on the average temperature in the vicinity of the exploding wire, the velocity of the shock waves generated, and the pressure behind the shock front. For example, the velocity of the shock waves observed in experiments with 100 μm diameter, 5 cm long copper wires exploded with currents of 40 kA in 70 ns is consistent with pressures of ∼50 GPa being formed near the expanding wire's surface, and spectral measurements suggest wire's temperatures of ∼5 eV are produced.[7] However, these methods above cannot provide direct information about how fast the wire itself expands nor its radial density profile and internal structure. The latter parameters are crucial for the validation of existing EOSs and conductivity models.

Radiography experiments on exploding wires in vacuum were carried out by Pikuz *et al.*[12–14] and showed a rapidly expanding wire with a highly heterogeneous structure in which only a fraction of the wire material was converted to plasma. Using optical diagnostics alone we would not be certain if the same processes occur in wires in water. The main advantage of underwater wire explosions as opposed to vacuum is the higher energy density deposition into the wire.
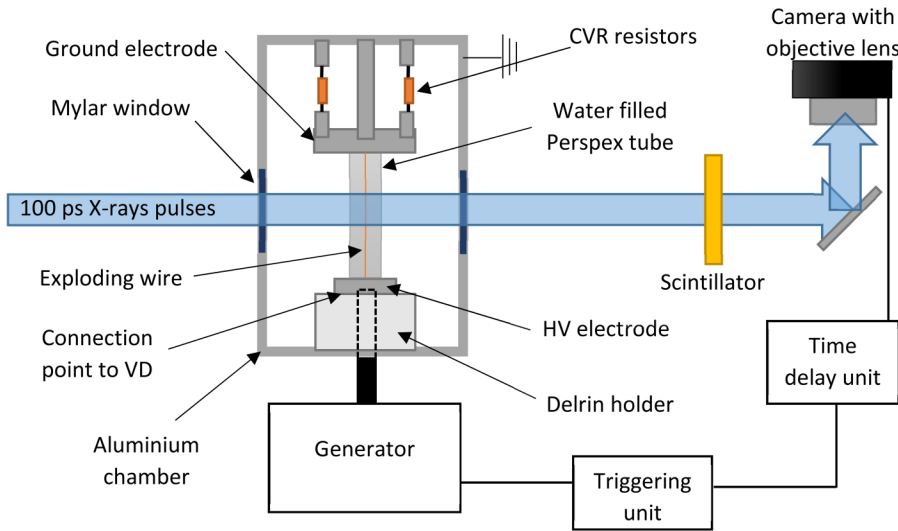
FIG. 1. Experimental setup.

This could, for instance, greatly alter the fraction of wire converted into plasma and may delay/prevent instability formation. Nitishinskiy *et al.* recently carried out x-ray radiography of copper wire experiments in water.[15] The x-ray source was based on a vacuum diode and photon energies above 60 keV were achieved. The 50-μm spatial resolutions achieved with temporal resolutions $\sim$20 ns enabled the density of the wire and its radius to be measured. However, these parameters of X-ray flux were insufficient to see any structure inside of the wire, nor could they observe the motion of the shock wave in the water generated by the wire's explosion.

In this paper, we present first x-ray radiography results of pulsed power driven, microsecond timescale, underwater copper and tungsten wire explosions performed at the European Synchrotron Radiation Facility (ESRF). The images obtained have much higher spatial and temporal resolutions than those in earlier experiments[15] and employ phase contrast imaging to highlight any edge effects—providing improved detail on the internal structure of the exploding wires, the expansion of the wires during implosion, and the shockwave launched into the water. The structure of the rest of the paper is as follows. In Sec. II, we describe the
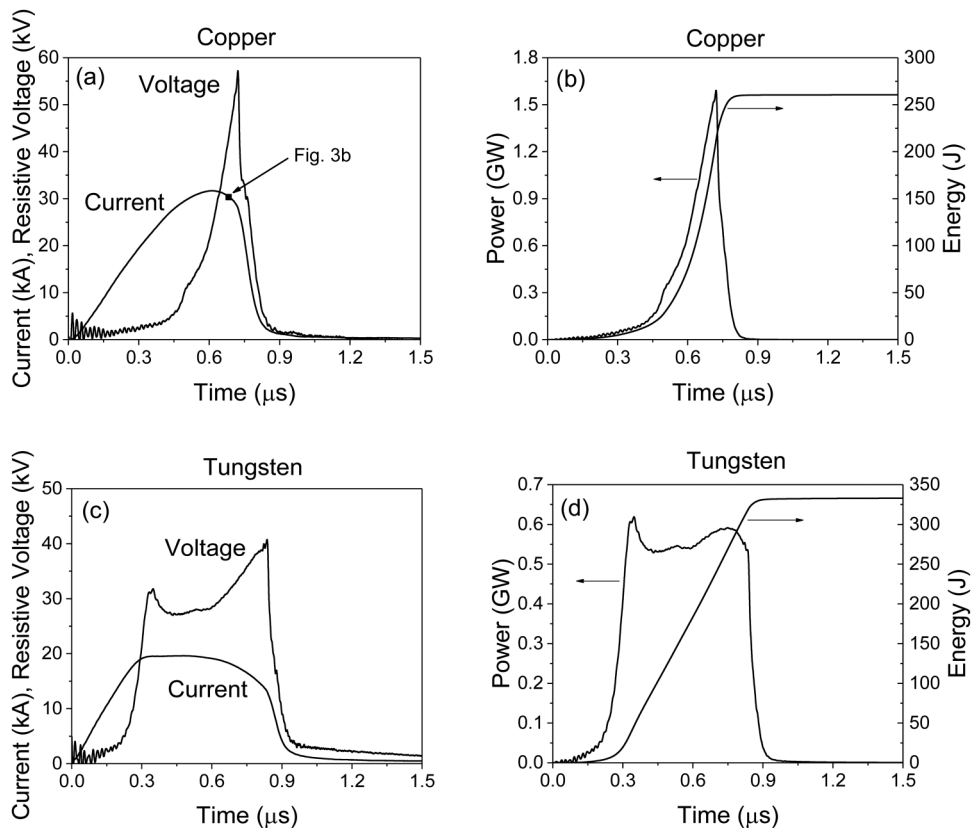
FIG. 2. Measured current and resistive voltage, and calculated power and energy input waveforms for copper [(a) and (b)] and tungsten [(c) and (d)] wires. [The marker in (a) is to clarify where the image in Fig. 3(b) is in time.]

experimental setup including details of the driver and the synchrotron probing radiation used. In Sec. III, results of copper and tungsten wire explosions are presented. These show instability growth in the exploding wire. In addition, we measure the expansion of the wire and the velocity of the shockwave launched directly from the radiographs to compare to 2D hydrodynamic (HD) simulations in Sec. IV. Abel inversion is used to determine the radial density profile of the exploding wires in Sec. V, and finally results and conclusion are presented in Sec. VI.

II. EXPERIMENTAL SETUP

Experiments were carried out using a compact pulsed power driver coupled to the ID19 beamline at the ESRF as shown in Fig. 1. The driver included 4 low-inductance high-voltage Maxwell capacitors of 220 nF each, connected in parallel, and triggered by a spark gas switch. The capacitors were charged to a voltage of 32 kV. The discharge current was measured by a current-viewing-resistor (CVR) of 0.021 Ω, and the voltage was measured using a Tektronix HV voltage divider.

Both copper and tungsten wires were used in the experiments, as these have been well explored in previous experiments, mainly through optical diagnostics.[7,12–15] The length of the wires was 45 mm, and the wire diameter of each material was chosen to be 200 μm, which critically damped current and maximised energy transfer to the wires. In practice, the wires were stretched and soldered between two electrodes which were screwed in an 8 mm inner diameter 1.5-mm-thick acrylic tube which was filled with deionized water. This setup was placed coaxially in a 98-mm diameter aluminum chamber, which provided the current return path and acted to contain any water spilled/debris produced during an experiment. Two 10 mm windows, covered in thin mylar foil, enabled the X-rays to pass through the chamber. This experimental setup is sketched in Fig. 1.

The ID19 beamline at the ESRF is located at a distance of 150 m from the undulators providing partially spatially coherent X-rays. The X-ray beam energy spectrum was polychromatic ranging from ~20 keV to ~50 keV with a mean energy of ~30 keV. The 4-bunch electron mode (704 ns between pulses) was used to produce a photon flux of ~3.7×10^7 photons/mm^2 before the chamber, with a pulse duration of 100 ps. Given the timescale of the experiment/ velocity of shock waves, this effectively acted to freeze any motion in the frame. After the sample, the beam was propagated another 5 m-10 m to obtain a propagation-based phase-contrast regime, where the interference of the diffracted waves increases the contrast at places with sharp changes in the refractive index.[16] After that, the beam hits an LYSO:Ce
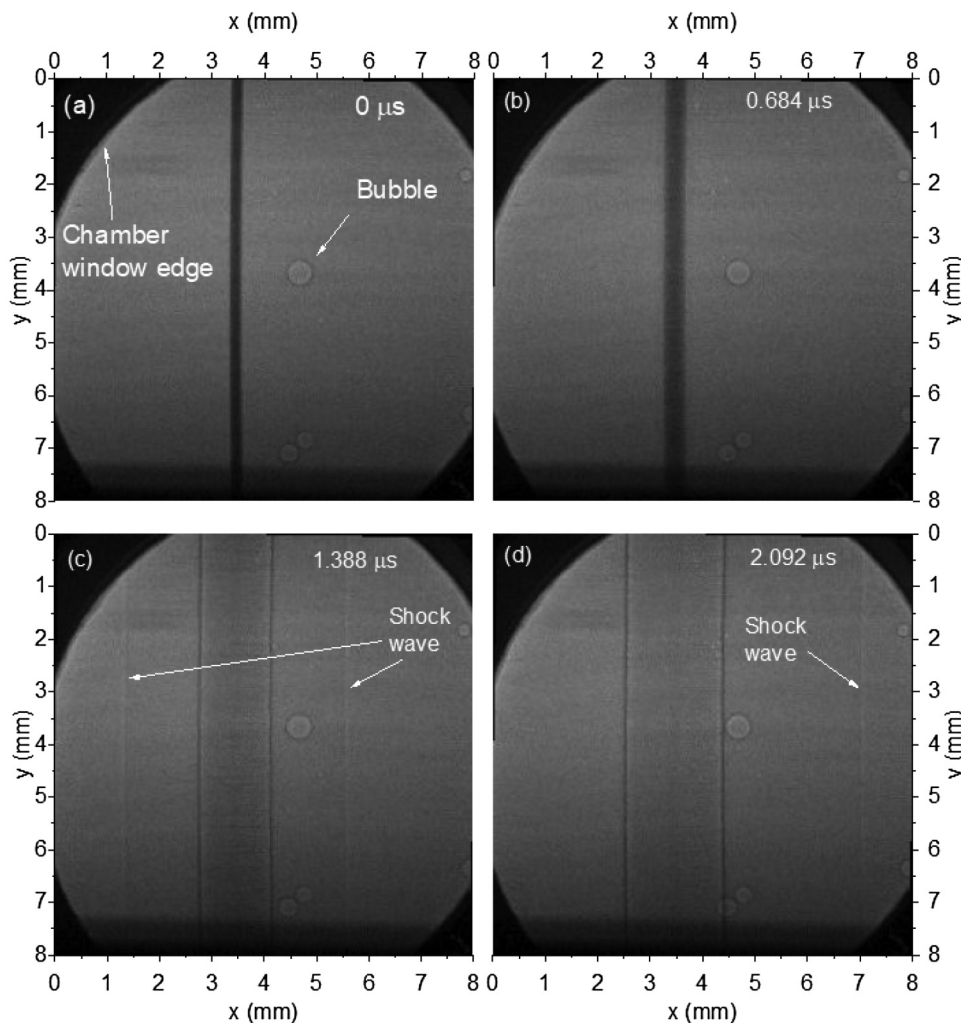
FIG. 3. Typical low-resolution images of an exploding copper wire.

scintillator imaged after a 45° mirror via a Shimadzu HPV-X2 camera using either a 1× or a 4× objective lens. Spatial resolution of the system was dominated by the pixel size at the detector and was 32 μm and 8 μm for low and high magnifications images, respectively. A more detailed description of the experimental setup of ID19 is available in Refs. 17 and 18. The x-rays were recorded by a fast photodiode and oscilloscope prior to the experiment along with a short-circuit load for synchronization, where ESRF radio frequency was used as a master clock.

III. EXPERIMENTAL RESULTS

The measured current through the wire, resistive voltage, along with the calculated power and energy input to the wire is shown in Fig. 2 for both tungsten and copper wire explosions. One can see that the current waveform for the copper wire explosion indicates a critically damped discharge. Initially, while the current in the copper rises, the wire heats up and undergoes phase transitions. The peak in the resistive voltage is obtained when the wire reaches maximum resistance ($\sim$2 Ω). One can see that the most energy density deposition occurs during $\sim$200 ns and a total energy of $\sim$260 J is deposited. The latter is far higher than the energy of $\sim$210 J that would be required to melt and vaporise the entire wire

and transfer it to a weakly-ionized plasma state. In the case of the tungsten wire, the current and voltage have a plateau with a duration of $\sim$600 ns, characterized by almost constant resistance ($\sim$1.5 Ω) of the exploding wire and during which almost $\sim$70% of the stored energy is delivered to the wire. Again, the energy deposited is far higher than the energy of $\sim$235 J required for the entire wire to melt, vaporise, and transfer it to a weakly-ionized plasma state. The long plateau was also observed in earlier research[19] and is likely due to a dwell in a mixed liquid-gas state because of its high density.

X-ray images of the exploding wires are presented in low (Figs. 3 and 4) and high (Figs. 5 and 6) spatial resolution. The time indicated in the images is the time delay from the beginning of the discharge current rise. One feature immediately noticeable on the radiographs is that the front of the shock wave can be resolved—this could not be observed in previous radiography experiments[15] and is primarily due to the enhancement of the sharp edge of the shock wave by phase contrast effects and due to shorter X-ray pulse width. We can also directly observe the water immediately behind the shock wave—in optical shadow imaging diagnostics, the shock wave scatters any backlighting radiation out of the system—only after several microseconds does the water turns clear again (see, for example, Fig. 5 in Ref. 8).
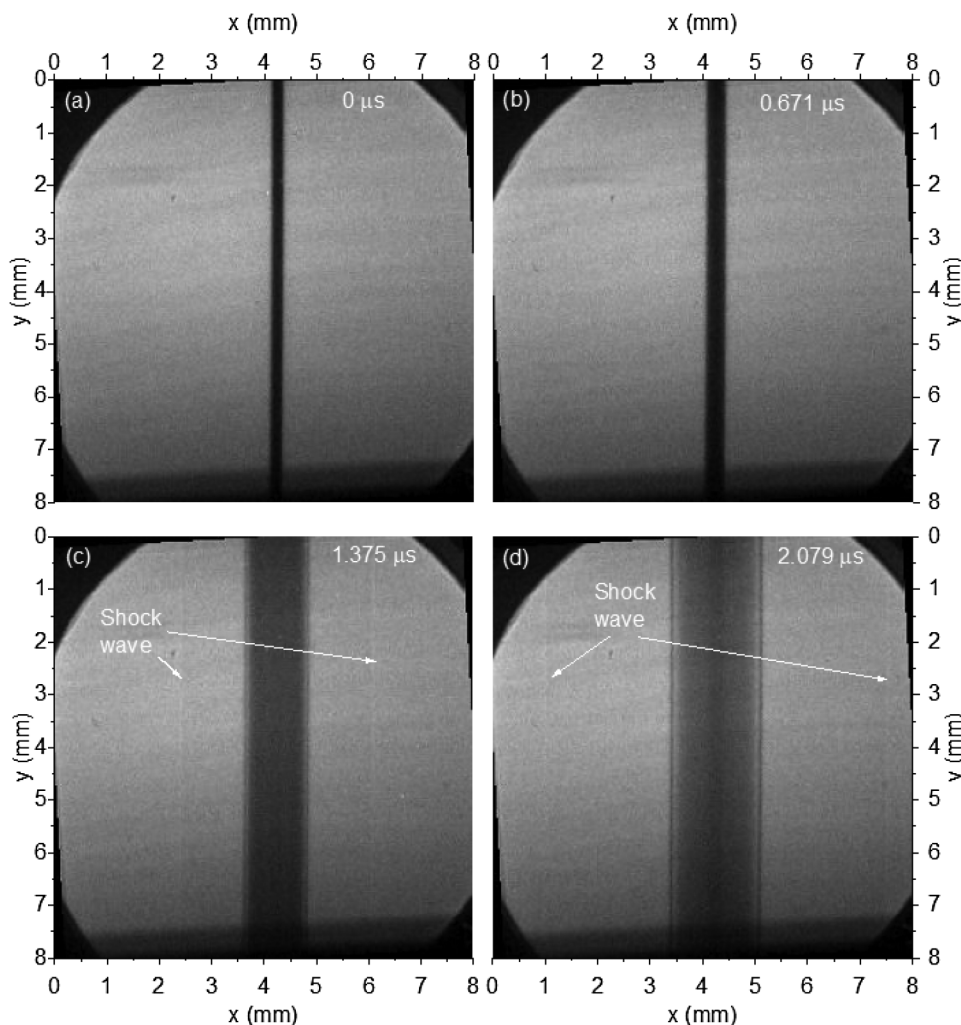
FIG. 4. Typical low-resolution images of an exploding tungsten wire.
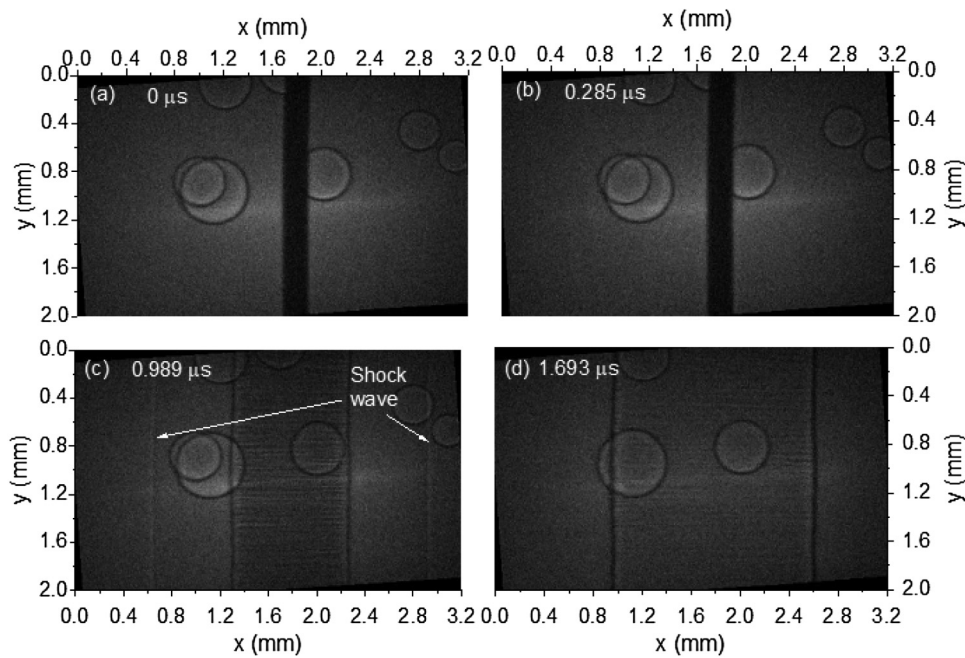
FIG. 5. Typical high-resolution images of an exploding copper wire.

In the radiography images, the boundary of the exploding wire with the water is also very clearly observed. Radiographs of the copper wire in Fig. 3 show the wire starts to expand around the time of peak current, which is when the vapor-weakly ionized plasma phase transition is expected to occur. This happens at a similar time for tungsten; however, there is no current peak at that time.

High resolution radiographs of the copper wire experiments revealed the presence of striations in the wire over the first ∼2-3 frames following the start of the expansion. The structure of these striations, clearly seen in Fig. 5(c), is possibly due to the same overheating instability thought to

contribute to the heterogeneous nature of wire explosions in vacuum.[20,21] This assumes microscopic regions of higher resistance in the wires that heat faster and so increase in resistance, shunting current into the adjacent material. This continues until an entire layer of the wire has been overheated. Simultaneously, the overheated layer will expand, and adjacent layers will then compress material between them reducing the resistance in this region so as to prevent overheating. The result is that along the wires, which are now in the weakly ionized plasma state, there are alternate layers of hot lower density and higher resistivity, and cold higher density and lower resistivity. It is unclear whether there are similar
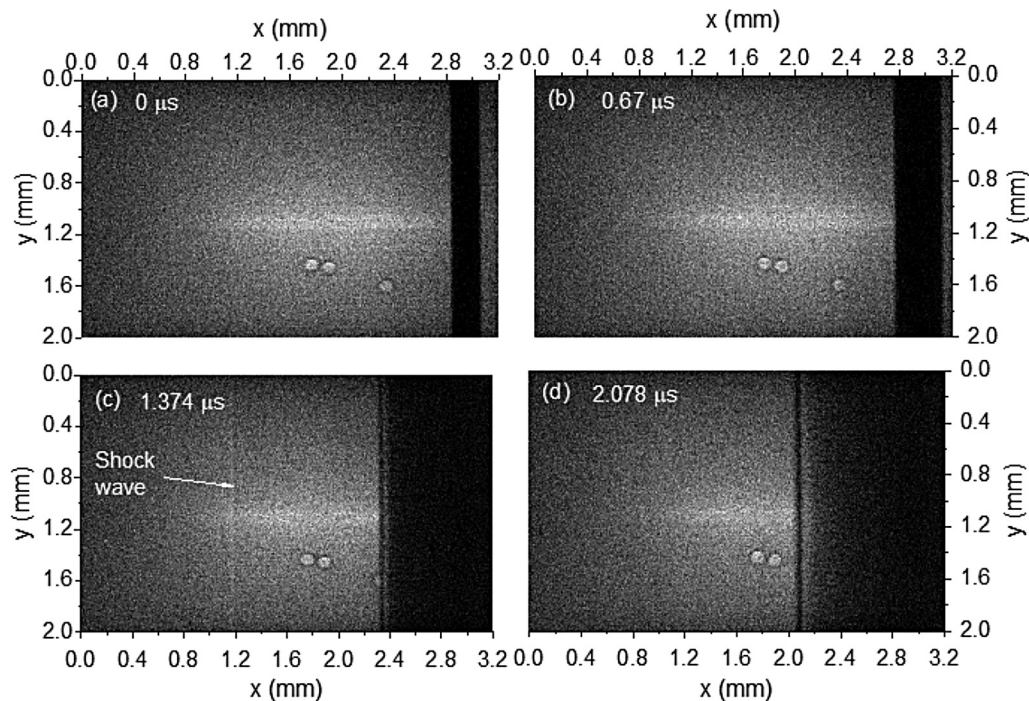
FIG. 6. Typical high-resolution images of an exploding tungsten wire.
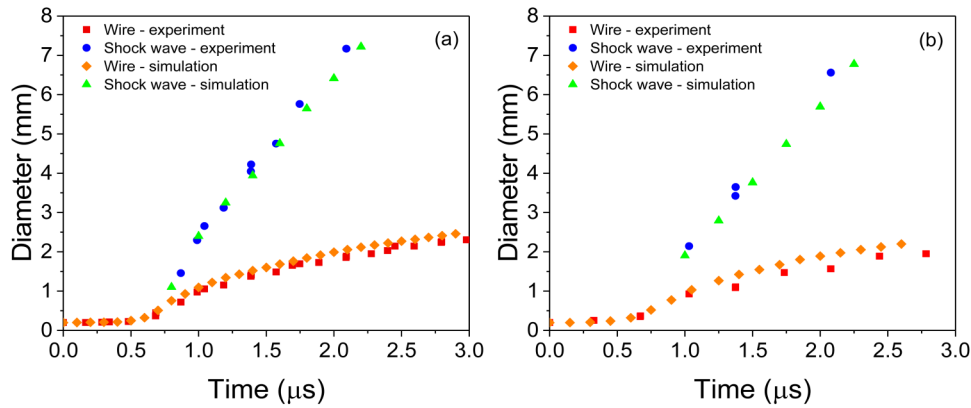
FIG. 7. Comparison between experimental and simulation diameters of the wire and position of the shock wave for (a) copper and (b) tungsten.

striations in tungsten wires—these could be obscured by the high areal density of tungsten and the striations could be on a much smaller spatial scale.

Despite the striations, the boundary of the exploding wire with the water appears remarkably straight and stable for the majority of the experiment. In some low magnification images (see Figs. 4c and 4d), a faint wire "core" can be seen at the original location of the wire. This was somewhat unexpected —in vacuum experiments, wire cores are seen surrounded by low density, ablating plasma. In the present experiments, the increased energy deposition into the wire was expected to produce a more uniform expansion. We suspect that this "core" is likely an artefact of the imaging system, enhanced by the large dynamic range of our experiment encompasses— going from essentially black (solid wire) to highly transparent. The scintillator used has a decay time of only ∼40 ns[17] which is much shorter than the time between X-ray pulses, 704 ns; however, this refers only to the first term in a series of decay factors.[22] There could be much longer-lived components that contribute to a faint background on the images. This suggestion is supported by the size of the wire "core" being the same as the initial wire diameter, $200 \mu m$, for shots with both tungsten and copper wires—despite these wires having different resistivities, thermal, and radiative properties. In high magnification images, where a different thickness scintillator was used, there is no obvious wire core present.

Using a combination of high and low-resolution images, both the expansion of the wire-water boundary and the position of the shock wave can be mapped. The low-resolution images have a smaller amount of noise and hence the clearer image, and because of the bigger area photographed, later images of the propagating shock waves could be acquired. However, the resolution is worse and small-scale effects are difficult to be seen. The high-resolution images have a better resolution but also a lot of shot-noise. In the following sections, we will use experimental measurements to compare to HD simulations of the expansion of the wire and launch of the shock wave and use the images directly to produce maps of density profiles via Abel inversion.

IV. COMPARISON OF RESULTS TO 2D HD SIMULATION

The experimentally measured positions of both the shock front and the water-wire boundary are shown in Fig. 7.

For both copper and tungsten wires, the average speed of the shock waves determined from radiography is ∼2.3 km/s and ∼2.1 km/s, respectively. These speeds are higher than earlier measurements made for a copper wire (1.57 km/s[23]) due to the higher value of power obtained (∼1.6 GW compared to ∼0.8 GW).

Negating the possible wire core, a simple 2D HD simulation is able to match both the expansion of the wire-water interface and the shock wave velocity. The simulation was based on three conservation laws, namely, mass, momentum, and energy conservation, using a Lagrangian mesh. These equations were coupled with water, copper, and tungsten EOSs.[24] The input to the simulation was the power calculated from the measured current and voltage in the experiment. Generally, in each time step, the power was input to the wire in the simulation and the conservation equations coupled with the EOSs were used to calculate the new pressure, temperature, and density, and the pressure gradient created caused the nodes in the Lagrangian mesh to move. In order to match the trajectory of the shock wave to the experimental results, only 80% of the input power was used in the simulations, which is consistent with earlier results.[10,11] This value of 80% of the input power could be related to several reasons. For instance, it can be explained by a part of the current flowing through the surrounding water, by slight overvaluation of the load inductance, since the inductance influencing the resistive voltage includes that of both the wire
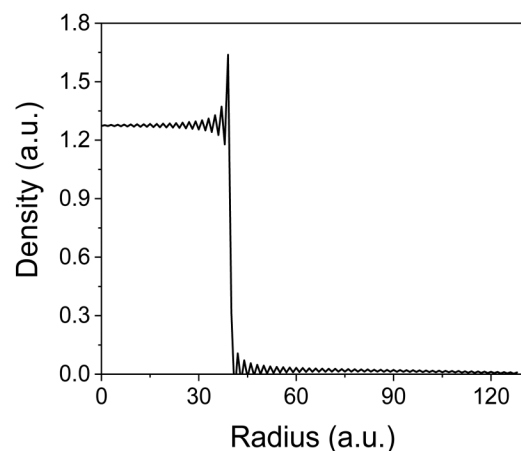
FIG. 8. Reconstruction of a perfect wire with uniform density using Abel inversion.
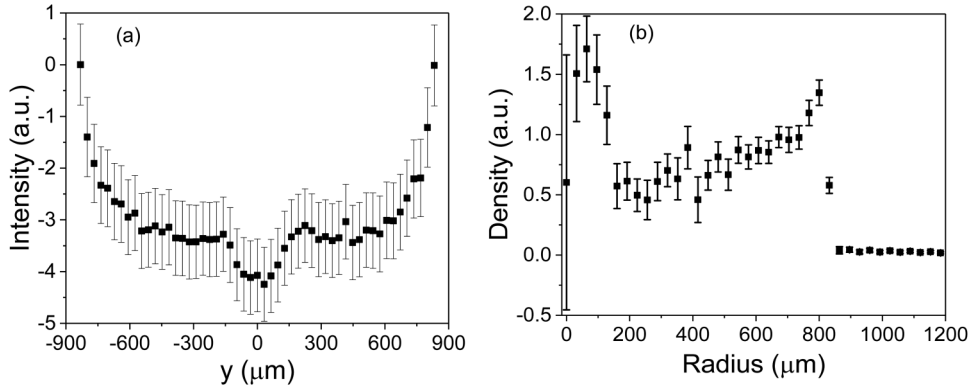
FIG. 9. (a) Absorption profile of the exploding copper wire at 2.092 μs delay from the beginning of the rise of the current, and (b) the Abel transform of this absorption profile.

and CVR, and lastly possible uncertainties in the EOS tables. A more detailed description of the algorithm used in the simulation is presented in Ref. 25. As one can see, the simulation and experimental results agree satisfactorily.

V. DENSITY PROFILE

Using Abel inversion, one can reconstruct a two-dimensional circularly symmetric function from its projection onto an axis. In our case, we reconstruct the wire's density $\rho(r)$, using the projection of X-rays onto the axis perpendicular to the wire $F(y) = 1/\bar{\mu} \ln [I_0/I(y)]$, where $\bar{\mu}$ is the X-ray mass absorption coefficient averaged across the x-ray wavelengths, I_0 is the measured background intensity, and $I(y)$ is the measured intensity behind the wire.[26] The reconstruction was performed in MATLAB using the Fourier-Hankel approach described in Ref. 27.

While the method used gives satisfactory results for high-resolution images with low dynamic range, the method magnifies experimental noise and produces artificial structures when reconstructing images with sharp features. For this reason, the results should be regarded as qualitative and not exact. Therefore, arbitrary units of the density were used for simplification. Still, the results are of much higher quality than obtained previously. To give the reader an idea of the effect of sharp edges, which we have in our experiment, a reconstruction of a theoretical perfect wire is presented in Fig. 8. As can be seen, the wire's edge introduces an artificial structure to the reconstruction.

With low magnification images, the lower average noise enabled good use of Abel inversion during the rapid expansion of the wire. The absorption profile of Fig. 3(d), averaged across the z axis (the axis along the wire), is presented in Fig. 9(a). This averaging could introduce a small error due to the very small bending radius of the wire. The baseline was taken to be zero, and the error bars are the standard error of the mean of all points along the z axis (250 points). The Abel inversion result of this absorption profile is presented in Fig. 9(b). The plot in Fig. 9(a) was padded with zeroes from both sides and the average was taken between the left and right halves of the image. To estimate the errors, the inversion was made to each line from the raw data and the standard error of the mean was taken from these inversions multiplied by 1.96 to get a confidence level of 95%.

The result for the tungsten wire is similar and, therefore, was not presented here.

One can see in Fig. 9 the effect of the faint wire core on the Abel inversion, producing a small increase in density at the original wire radius. As discussed in Sec. II, this feature is likely not real, and an artefact of the imaging system. In case this is a real result, it is magnified further by the process of the inversion. As can be seen in Fig. 8, sharp edges introduce numerical artefacts to the inversion; therefore, the real density in the denser region is lower than suggested by Fig. 9(b) (roughly ∼30% higher than the surrounding plasma).

We explored the possibility of the core being real through the use of one dimensional magnetohydrodynamic (MHD) simulations. While the 2D HD simulations in Sec. IV model a uniform explosion of a wire given a total energy into the system, emphasizing the generated shock wave in water, the production of a wire core would however require a non-uniform current density distribution inside the wire. The model which is described in detail in Ref. 28 included the standard MHD equations accounting heat transfer, mass, energy, and momentum conservation equations, Maxwell equations, Ohm's law coupled with EOS[24] of copper and water, and using an electrical conductivity model.[29] Results of this simulation are shown in Fig. 10. Despite the more complicated model's capabilities, it was unable to reproduce production of a wire core given any
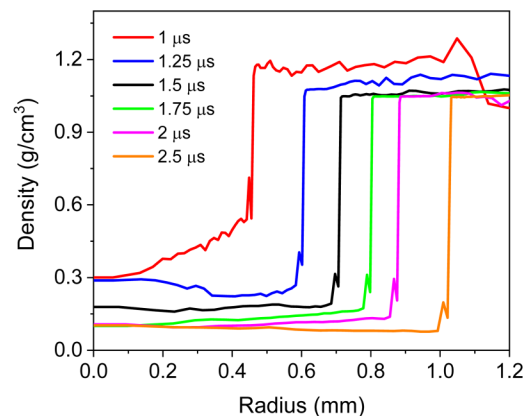
FIG. 10. Radial density distribution of an exploding copper wire obtained by MHD simulation (The plateaus to the right, ∼1 g/cm³, are water surrounding the wire).
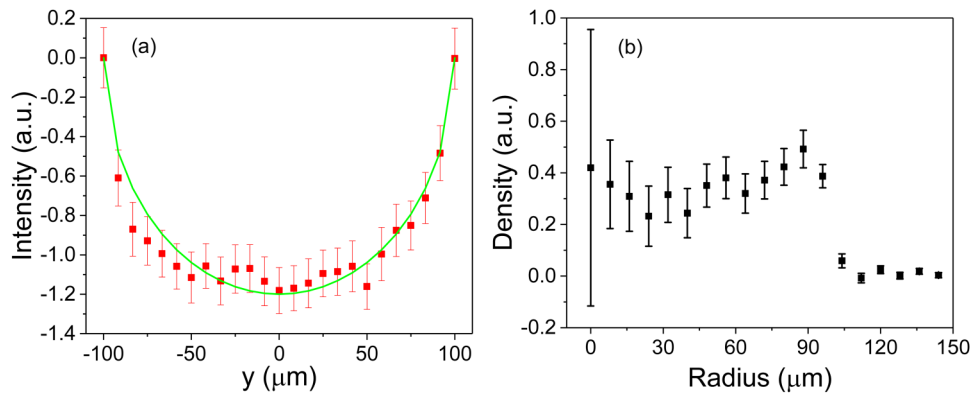
FIG. 11. (a) Absorption profile of a copper wire before explosion along with the theoretical curve. (b) Inverse Abel transform of the wire before explosion.

reasonable set of input parameters from the experiment, supporting our suspicion it is an imaging artefact. This will be explored in future experiments at the ESRF, after the upgrades to the facility over 2019-2020.

Abel inversion of the high magnification images was also attempted. Here, we have more resolution; however, the level of the noise is large, and so the error bars of the inversion result are larger. Here, only the absorption profile and inversion of the wire before the explosion is presented (Fig. 11) with comparison to the theoretical profile to give a rough estimate of the noise levels and their effect and to give an example of the quality of the radiographs obtained to provide expectations from future experiments. As opposed to Fig. 9(a), 1.96 times the standard error of the mean was taken in Fig. 11(a) to try to fit to the theoretical line. As can be seen, even with a 95% confidence level, a straight line (uniform density) could not fit to the inverse Abel transform in Fig. 11(b). This procedure could not be carried out for tungsten because it absorbed all the beam except for the edges of the wire.

VI. SUMMARY

Synchrotron based X-ray radiography experiments of pulsed power driven copper and tungsten wire explosions have been carried out for the first time, allowing direct imaging of the wires' internal structure along with its expansion and the velocity of the shock wave to be obtained in the same experiment.

Radiography images show that the significant expansion of the wires only starts at peak current when the wire is expected to undergo phase transformations into the dense and weakly-ionised plasma. The boundary of the wire/water expansion is relatively uniform; however, in copper wire experiments, the wire material inside this boundary develops a highly heterogeneous structure, with radial striations possibly due to the overheat instability.

The expansion of the wire and the velocity of the shock wave launched into the water were measured with a high degree of resolution. The velocity of the shock waves from both tungsten and copper wires agreed with earlier data from optical diagnostics. Abel inversion based density profiles could be made from low noise. Finally, 2D simulations of the wires and shock waves were performed, and the calculations compared well to experimental data.

On some of the images, a faint "wire core" appeared to be present. This, we suspect is an artefact of the imaging system—however, it will be explored in future research.

[1]E. A. Martin, "Experimental investigation of a high-energy density, high-pressure arc plasma," J. Appl. Phys. **31**, 255 (1960).
[2]H. Goronkin, "Striations in fast wire explosions," J. Appl. Phys. **39**, 5345 (1968).
[3]J. W. Robinson, M. Ham, and A. N. Balaster, "Ultraviolet radiation from electrical discharges in water," J. Appl. Phys. **44**, 72 (1973).
[4]W. M. Lee and R. D. Ford, "Pressure measurements correlated with electrical explosion of metals in water," J. Appl. Phys. **64**, 3851 (1988).
[5]A. W. DeSilva and J. D. Katsouros, "Electrical conductivity of dense copper and aluminum plasmas," Phys. Rev. E **57**, 5945 (1998).
[6]B. Liu, D. Wang, and Y. Guo, "Influence of water conductivity on shock waves generated by underwater electrical wire explosion," Phys. Lett. A **382**, 49 (2018).
[7]A. Grinenko, Y. E. Krasik, S. Efimov, A. Fedotov, V. T. Gurovich, and V. I. Oreshkin, "Nanosecond time scale, high power electrical wire explosion in water," Phys. Plasmas **13**, 042701 (2006).
[8]A. Grinenko, S. Efimov, A. Fedotov, Y. E. Krasik, and I. Schnitzer, "Efficiency of the shock wave generation caused by underwater electrical wire explosion," J. Appl. Phys. **100**, 113509 (2006).
[9]S. Efimov, V. T. Gurovich, G. Bazalitski, A. Fedotov, and Y. E. Krasik, "Addressing the efficiency of the energy transfer to the water flow by underwater electrical wire explosion," J. Appl. Phys. **106**, 073308 (2009).
[10]S. N. Bland, Y. E. Krasik, D. Yanuka, R. Gardner, J. MacDonald, A. Virozub, S. Efimov, S. Gleizer, and N. Chaturvedi, "Generation of highly symmetric, cylindrically convergent shockwaves in water," Phys. Plasmas **24**, 082702 (2017).
[11]D. Yanuka, A. Rososhek, S. Efimov, M. Nitishinskiy, and Y. E. Krasik, "Time-resolved spectroscopy of light emission from plasma generated by a converging strong shock wave in water," Appl. Phys. Lett. **109**, 244101 (2016).
[12]S. A. Pikuz, T. A. Shelkovenko, A. R. Mingaleev, D. A. Hammer, and H. P. Neves, "Density measurements in exploding wire-initiated plasmas using tungsten wires," Phys. Plasmas **6**, 4272 (1999).
[13]D. B. Sinars, T. A. Shelkovenko, S. A. Pikuz, M. Hu, V. M. Romanova, K. M. Chandler, J. B. Greenly, D. A. Hammer, and B. R. Kusse, "The

effect of insulating coatings on exploding wire plasma formation," Phys. Plasmas **7**, 429 (2000).

[14]S. A. Pikuz, T. A. Shelkovenko, D. B. Sinars, J. B. Greenly, Y. S. Dimant, and D. A. Hammer, "Multiphase foamlike structure of exploding wire cores," Phys. Rev. Lett. **83**, 4313 (1999).

[15]M. Nitishinskiy, D. Yanuka, A. Virozub, and Y. E. Krasik, "Radial density distribution of a warm dense plasma formed by underwater electrical explosion of a copper wire," Phys. Plasmas **24**, 122703 (2017).

[16]A. Snigirev, I. Snigireva, V. Kohn, S. Kuznetsov, and I. Schelokov, "On the possibilities of x-ray phase contrast microimaging by coherent high-energy synchrotron radiation," Rev. Sci. Instrum. **66**, 5486 (1995).

[17]M. P. Olbinado, X. Just, J. Gelet, P. Lhuissier, M. Scheel, P. Vagovic, T. Sato, R. Graceffa, J. Schulz, A. Mancuso, J. Morse, and A. Rack, "MHz frame rate hard X-ray phase-contrast imaging using synchrotron radiation," Opt. Express **25**, 13857 (2017).

[18]M. P. Olbinado, V. Cantelli, O. Mathon, S. Pascarelli, J. Grenzer, A. Pelka, M. Roedel, I. Prencipe, A. L. Garcia, U. Helbig, D. Kraus, U. Schramm, T. Cowan, M. Scheel, P. Pradel, T. De Resseguier, and A. Rack, "Ultra high-speed x-ray imaging of laser-driven shock compression using synchrotron light," J. Phys. D Appl. Phys. **51**, 055601 (2018).

[19]R. Han, J. Wu, H. Zhou, W. Ding, A. Qiu, T. Clayson, Y. Wang, and H. Ren, "Characteristics of exploding metal wires in water with three discharge types," J. Appl. Phys. **122**, 033302 (2017).

[20]A. G. Rousskikh, V. I. Oreshkin, S. A. Chaikovsky, N. A. Labetskaya, A. V. Shishlov, I. I. Beilis, and R. B. Baksht, "Study of the strata formation during the explosion of a wire in vacuum," Phys. Plasmas **15**, 102706 (2008).

[21]V. I. Oreshkin, R. B. Baksht, N. A. Ratakhin, A. V. Shishlov, K. V. Khishchenko, P. R. Levashov, and I. I. Beilis, "Wire explosion in vacuum: Simulation of a striation appearance," Phys. Plasmas **11**, 4771 (2004).

[22]M. E. Rutherford, D. J. Chapman, T. G. White, M. Drakopoulos, A. Rack, and D. E. Eakins, "Evaluating scintillator performance in time-resolved hard X-ray studies at synchrotron light sources," J. Synchrotron Rad. **23**, 685 (2016).

[23]D. Yanuka, A. Rososhek, and Y. E. Krasik, "Comparison of electrical explosions of Cu and Al wires in water and glycerol," Phys. Plasmas **24**, 053512 (2017).

[24]S. P. Lyon and J. D. Johnson, *The Los Alamos National Laboratory Equation-of-State Database*, LANL Report No. LA UR-92-3407, 1992.

[25]M. Kozlov, V. T. Gurovich, and Y. E. Krasik, "Stability of imploding shocks generated by underwater electrical explosion of cylindrical wire array," Phys. Plasmas **20**, 112701 (2013).

[26]H. R. Griem, *Principles of Plasma Spectroscopy* (Cambridge University Press, Cambridge, 1997).

[27]L. M. Smith, D. R. Keefer, and S. I. Sudharsanan, "Abel inversion using transform techniques," J. Quant. Spectrosc. Radiat. Transfer **39**, 367 (1988).

[28]A. Grinenko, V. T. Gurovich, A. Saypin, S. Efimov, and Y. E. Krasik, "Strongly coupled copper plasma generated by underwater electrical wire explosion," Phys. Rev. E **72**, 066401 (2005).

[29]Yu. D. Bakulin, V. F. Kuropatenko, and A. V. Luchinskii, Sov. Phys. Tech. Phys. **21**, 1144 (1976).